Remote Sensing Applications: Society and Environment 30 (2023) 100951

Contents lists available at ScienceDirect

Remote Sensing Applications: Society and Environment

journal homepage: www.elsevier.com/locate/rsase

Application of machine learning techniques to derive sea water turbidity from Sentinel-2 imagery

Stefania Magrì [a, b, *], Ennio Ottaviani [c, d], Enrico Prampolini [c], Giovanni Besio [a], Bruno Fabiano [a], Bianca Federici [a]

[a] UNIGE, Civil, Chemical and Environmental Engineering Department (DICCA), Via Montallegro 1, 16145, Genoa, Italy
[b] Regional Agency for the Environmental Protection of Liguria (ARPAL), Via Bombrini 8, 16149, Genoa, Italy
[c] OnAIR s.r.l., Via Carlo Barabino 26, 16129, Genoa, Italy
[d] UNIGE, Department of Mathematics (DIMA), Via Dodecaneso 35, 16136, Genoa, Italy

ARTICLE INFO

Keywords:
Turbidity
Sentinel-2
Machine learning
Water quality
Satellite remote sensing

ABSTRACT

Earth Observation (EO) from satellites has the potential to provide comprehensive, rapid and inexpensive information about water bodies, integrating in situ measurements. Traditional methods to retrieve optically active water quality parameters from satellite data are based on semi-empirical models relying on few bands, which often revealed to be site and season specific. The use of machine learning (ML) for remotely sensed water quality estimation has spread in recent years thanks to the advances in algorithm development and computing power. These models allow to exploit the wealth of spectral information through more flexible relationships and are less affected by atmospheric and other background factors. The present study explores the use of Sentinel-2 MultiSpectral Instrument (MSI) Level-1C Top of Atmosphere spectral radiance to derive water turbidity, through application of machine learning techniques. A dataset of 222 combination of turbidity measurements, collected in the North Tyrrhenian Sea – Italy from 2015 to 2021, and values of the 13 spectral bands in the pixel corresponding to the sample location was used. Two regression techniques were tested and compared: a Stepwise Linear Regression (SLR) and a Polynomial Kernel Regression. The two models show accurate and similar performance (R^2 = 0.736, RMSE = 2.03 NTU, MAE = 1.39 NTU for the SLR and R^2 = 0.725, RMSE = 2.07 NTU, MAE = 1.40 NTU for the Kernel). A band importance analysis revealed the contribution of the different spectral bands and the main role of the red-edge range. The work shows that it is possible to reach a good accuracy in turbidity estimation from MSI TOA reflectance using ML models, fed by the whole spectrum of available bands, although the possible generation of errors related to atmospheric effect in turbidity estimates was not evaluated. Comparison between turbidity estimates obtained from the models with turbidity data from Copernicus CMEMS dataset named 'Mediterranean Sea, Bio-Geo-Chemical, L3, daily observation' produced consistent results. Finally, turbidity maps from satellite imagery were produced for the study area, showing the ability of the models to catch extreme events.

* Corresponding author. UNIGE, Civil, Chemical and Environmental Engineering Department (DICCA), Via Montallegro 1, 16145 Genoa, Italy.
E-mail address: stefania.magri@edu.unige.it (S. Magrì).

https://doi.org/10.1016/j.rsase.2023.100951
Received 5 December 2022; Received in revised form 23 February 2023; Accepted 6 March 2023
Available online 8 March 2023

1. Introduction

Turbidity is a measure of the amount of light scattered by suspended particles in water, i.e. suspensoids, operationally defined as the fraction which can be removed by a 0.22 μm (or 0.45 μm) -pore size filter (Kirk, 1985). Suspensoids include plankton and inanimate, organic or inorganic, particles. Even though algal blooms can seasonally be observed, in the coastal marine environment high turbidity events are dominated by suspended sediments: sediment load from rivers runoff, sea bottom resuspension due to wave action, shoreline erosion, anthropogenic activities that cause the resuspension or load of fine sediments, such as beach nourishment, coastal infrastructures, dredging activities. It is widely recognised that the increase of suspended solid concentration can determine negative environmental effects on the marine ecosystem (Erftemeijer et al., 2012; Wilber and Clark, 2001). In coastal marine systems at a high level of anthropization, sediments may contain toxic substances: heavy metals, polycyclic aromatic hydrocarbons (PAHs), tributyltin (TBT), polychlorinated (Garbolino et al., 2014). Sediments thus represent a potential source of contaminants whose resuspension and dispersion under different hydrodynamics conditions can contribute to propagate pollution (Lisi et al., 2019; Magrì et al., 2020). Additionally, as a result of climate change, extreme weather events are expected to occur more frequently, increasing coastal and soil erosion susceptibility, generating high levels of sediments and turbidity in rivers and coastal waters.

Many marine water quality monitoring programmes of EU legislation require to measure nephelometric turbidity for its significant direct and indirect effects on aquatic ecosystems (Zampoukas et al., 2013). However, according to OSPAR (OSPAR Commission, 2008), monitoring activity still lacks coordination and data sharing among the different programmes and the involved institutes. The accurate, but punctual and sparse, information provided by traditional sampling methods could gain in effectiveness if integrated with approaches that are able to collect data from wide geographic areas (Zampoukas et al., 2012). Remote sensing from satellites offers observations of the sea surface over large areas in a cost-effective way, as an always increasing amount of data can freely be accessed through specific websites. Water quality retrieval from satellites has gained recognition as a valid integrative tool for monitoring water bodies with the availability of new imagery from optical multispectral sensors with a higher spatial, spectral, and temporal resolution, like those of Landsat and Sentinel-2.

Ocean colour is primarily governed by Chlorophyll (Chl-a) and any of its accessory pigments in open sea, while in inland and coastal waters, the colour is further modulated by the presence of organic and inorganic particles and dissolved matter (Pahlevan et al., 2020).

Commonly used methods to estimate turbidity from satellite images are based on semi-empirical algorithms relying on water reflectance in bands that have shown the highest physical correlation to the parameter, also combined as band ratios. For low concentration of suspended sediments, turbidity is mostly related to water reflectance in the green and red parts of the spectrum. Red reflectance is more sensitive than green reflectance in medium-high turbid waters, while for sediment dominated highly turbid waters, a saturation of the water reflectance in the green and red bands is usually observed, so a NIR band is usually more appropriate (Doxaran et al., 2002b). A Normalized Difference Turbidity Index (NDTI), defined as (Red - Green)/(Red + Green), is often used to estimate the turbidity in inland water bodies (Baughman et al., 2015).

Terra and Aqua Moderate Resolution Imaging Spectroradiometer (MODIS) spectral data have been successfully applied to retrieve turbidity and suspended particulate matter (SPM) in coastal and estuarine environments (Doxaran et al., 2002, 2009; Chen et al., 2007; Miller and McKee, 2004; Petus et al., 2010; Hudson et al., 2017). Numerous studies reported effective ways to utilize medium-resolution Landsat Thematic Mapper (TM), Enhanced Thematic Mapper Plus (ETM +), Operational Land Imager (OLI) and Sentinel-2 MultiSpectral Instrument (MSI) sensors images for inland waters, lagoon, marshes and estuarine coastal waters (Akbar et al., 2014; Nas et al., 2010; Liu and Wang, 2019; Pereira et al., 2018; Quang et al., 2017; Joshi et al., 2017; Baughman et al., 2015; Bustamante et al., 2009; Abirhire et al., 2020; Katlane et al., 2020; Caballero et al., 2018).

Despite their good general performance, these types of models are dependent on reflectance ranges and turbidity levels, therefore their validity and accuracy often reveal to be limited to the domain (Dogliotti et al., 2015) and season (Joshi et al., 2017) over which they have been developed. This often leads in practice to site-specific models whose coefficients need to be locally adapted for a defined coastal domain (Han et al., 2016). Hence, it is difficult to select one model that will provide accurate turbidity retrieval from low to high-turbidity waters, limiting the application of studies over large coastal areas.

For this reason, geographically weighted regression (GWR) and geographically and temporally weighted regression (GTWR) models have been proposed in literature (Chu et al., 2018) to take into consideration spatio-temporal variation in model coefficients.

Nechad et al. (2010) proposed a multi conditional single band algorithm for SPM in estuarine coastal environments, based on red band for medium-low turbidity waters and NIR band in highly turbid waters. The difficulty resides in the selection of the limiting bounds for each model. The algorithm scheme has been applied with robust results to many studies in coastal and estuarine environments, where the switching thresholds is based on ranges of turbidity/SPM concentration (Feng et al., 2014) or reflectance values (Dogliotti et al., 2015; Han et al., 2016; Novoa et al., 2017; Caballero et al., 2018).

The automated switching algorithm described in Novoa et al., (2017) constitutes the basis for the turbidity data, expressed in FNU, obtained from the Sentinel-2 MSI sensor and introduced into Copernicus Marine Service website in May 2021, named 'Mediterranean Sea, Bio-Geo-Chemical, L3, daily observation' (https://data.marine.copernicus.eu/).

An alternative approach to semi-empirical models is provided by nonparametric regression, where no explicit relationship between reflectance and the parameter of interest is assumed, but the functional form is inferred from the data. Very flexible relations can be accommodated, responding to the need of a model that can adapt to varying water conditions with smooth transition, and the wealth of spectral information can be exploited. Ruescas et al. (2018) applied and compared five ML methods to Sentinel-2 MSI and Sentinel-3 OLCI simulated reflectance data for the retrieval of Colored Dissolved Organic Matter (CDOM), showing that best results were obtained when all bands from visible to NIR together with band ratios were used as input of non-linear ML models. Similarly, a

neural network (NN) model was developed by Chebud et al. (2012) to quantify Chl-a, turbidity and phosphorus from reflectance values from the seven Landsat TM bands, including SWIR and thermal bands. El Din (2019) showed, through application of Principal Components Analysis (PCA), that also Coastal Aerosol band provides important information in high turbid waters. Pahlevan et al. (2020) introduced a Mixture Density Network (MDN) approach for estimations of Chl-a from seven MSI and twelve OLCI bands, that largely outperforms existing algorithms when applied across different bio-optical regimes in inland and coastal waters. Similarly, Peterson et al. (2020) applied NN Deep learning (NNs) model fed by seven raw harmonized Landsat-8 and Sentinel-2 (HLS) spectral bands, from Coastal Aerosol to SWIR-2, supplemented with a series of additional spectral features to add key information based on standard band ratios method for the estimation of blue-green algae (BGA), Chl-a, fluorescent dissolved organic matter (fDOM), dissolved oxygen (DO), specific conductance (SC), and turbidity in inland waters. Application of ML algorithms seems to be promising for the retrieval of optically active parameters when investigating wide areas or long time series that include different optical water types and is thus the focus of this study. The present work explores the use of the whole spectrum of Sentinel-2 MSI bands, applying a Stepwise Linear Regression (SLR) and a Polynomial Kernel Regression, to estimate turbidity in an area on the North Tyrrhenian Sea that covers the Cinque Terre Marine Protected Area on the east side of the Liguria Sea, until Livorno harbour in Tuscany, based on in situ data representative of a wide range of turbidity conditions, covering a period from 2015 to 2021.

While physically-based relationships require robust atmospheric correction (AC), which is the process to remove the effect of absorption and scattering due to the constituent particles of the atmosphere, to obtain Bottom Of Atmosphere (BOA) reflectance, ML algorithms are less affected by the atmospheric and other background factors (Chebud et al., 2012). Inaccurate AC leads to large uncertainties in satellite data products, with effects on quantitative retrieval of optically active water quality parameters (Pahlevan et al., 2020). As a result, some satellite-based methods for the detection, for instance, of Sea Surface Salinity (Medina-Lopez, 2020) or Harmful Algal Blooms (Binding et al., 2021) rely on Level-1 TOA quantities in order to avoid large uncertainties in Level-2 BOA products introduced by poor AC.

The Atmospheric Correction Intercomparison Exercise, ACIX-Aqua (Pahlevan et al., 2021), examined the performance of eight state-of-the-art AC methods available for Landsat-8 and Sentinel-2 data processing over lakes, rivers, and coastal waters. The work highlights that performance of the different methods depends on optical water type, and that best-performer's uncertainties across the different bands are not uniform. Finally, the work attempted to evaluate how uncertainties in AC impact on Chl-a and SPM retrieval. The work reveals that despite high improvement in processors available, AC over inland and coastal waters remains one of the major challenges in aquatic remote sensing.

As no atmospheric parameters, coherent in space and time with the processed images, are available for the present study (Pisanti et al., 2022) and no in-situ optical data is available to support the choice of an AC algorithm, the 13 Level-1C TOA spectral bands were chosen to train the predictive models. The study aims at: i) investigating the possible use of TOA and ii) explore the use of the whole spectrum of available bands to increase the accuracy and flexibility of the models, through application of ML algorithms.

2. Material and methods

2.1. The study area

The research area is located in the North Tyrrhenian Sea – Italy (Fig. 1), covering a coastline of about 100 km, characterized by a varied shoreline, embracing environments worthy of protection and valuable biodiversity, including Cinque Terre Marine Protected Area, aquaculture and shellfish farms, the Versilia extensive sandy shoreline with a strong tourist vocation, but also relevant ports such as Livorno and La Spezia. Two main rivers flow in the area with a significant sediment discharge: Magra River, whose basin covers an area of about 1700 km^2 and separates Liguria and Tuscany regions, with an average flow of about 40 m^3/s; Arno River, which

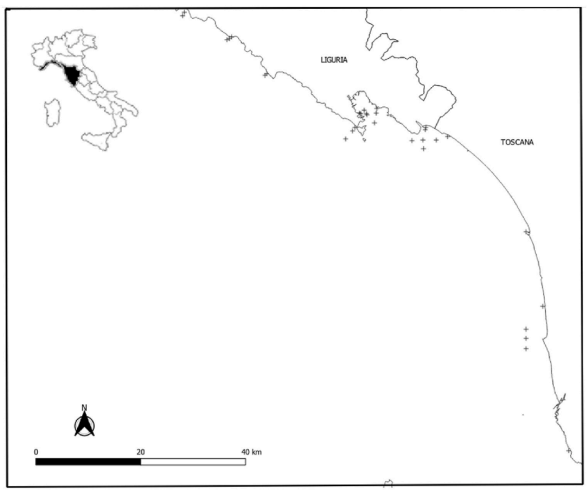

Fig. 1. Study area and distribution of the sampling stations.

represents the main watercourse in Tuscany and the second largest Apennine river in Italy, with a basin of about 8200 km^2 and an estimated average annual discharge of approximately 110 m^3/s. The coastal environment in this area has been monitored since 2001, according to the 2000/60/EC Water Framework Directive (WFD), and in 2008 EU Marine Strategy Framework Directive 2008/56/EC (MSFD) further strengthened the investigation in the area, resulting in 31 monitoring stations located along the coast. Water quality monitoring includes physical and chemical parameters along the water column and in sediments.

2.2. Turbidity measurements

For the present study, in-situ data collected according to the WFD and MSFD by the Regional Environmental Agencies ARPAL (Liguria Region) and ARPAT (Toscana Region), from April 2015 to December 2021, in the 31 stations located in the area (Fig. 1) were used. Turbidity was measured using a multi-parameter probe, together with electrical conductivity, temperature, salinity, and pressure of seawater. Turbidity was measured in nephelometric turbidity units (NTU), a measure of the amount of light scattered by particles at right angles to an incident beam of white light. At each station, turbidity profiles were conducted from the surface to the sea bottom, by lowering the probe at a rate of 1 m per minute with values recorded every second. To obtain a good representation of surface turbidity that is consistent for each station, the average turbidity at 0.5 m was used. The different monitoring stations have a specific sampling frequency according to the reference Directive, therefore on-site measurements are not available for all stations on the same days, but mostly for groups of stations.

Out of 234 day of field campaigns in the area, only 84 had a corresponding satellite overpass, corresponding to 394 co-located pairs of turbidity records and reflectance, that were further analysed. Available measures include a variety of turbidity conditions (clean water, algal blooms, river discharge events), with turbidity values ranging from 0.1 to 28.7 NTU. The complete histogram of measured turbidity data distribution is shown in Fig. 2, highlighting the predominance of low turbidity values. It should be remarked that higher turbidity conditions often correspond to extreme, or at least intense, meteorological events, not suitable for in situ sampling and indeed associated to high cloudiness, when optical satellite images do not provide useful information.

2.3. Image acquisition and pre-processing

For the present work, the Sentinel-2 MSI optical images have been processed, freely downloaded from Copernicus Open Access Hub website. Sentinel-2 is composed of two identical satellites 2A and 2B, launched in June 2015 and March 2017, respectively, by the European Space Agency (ESA). The two satellites, placed on the same orbit but phased at 180°, allow to acquire images about every 2–5 days at the latitudes of the area of interest. The MultiSpectral Instrument mounted on Sentinel-2 covers 13 spectral bands from visible to short-wave infrared wavelengths, from 10 to 60 m spatial resolution, and orbit swath widths of up to 290 km (ESA website). Image stacks of 13 bands are generated in spatial tiles, ortho-images in WGS84/UTM projection, each one covering an area of approximately 100x100 Km.

For the study, tile T32TNP was used, which covers the entire study area with a single image stack. An example of the T32TNP tile is presented in Fig. 3 (October 8th, 2020), using a True Colour Image (TCI) built from the bands B02 (Blue), B03 (Green) and B04 (Red).

Since March 2018, the Sentinel-2 processing pipeline produces both Level-1C TOA and Level-2A BOA products, the latter including atmospheric correction performed by the specific image processor Sen2Cor. However, AC over inland and coastal waters requires the use of methods specifically designed for the purpose, that should be selected according to the optical water type (Pahlevan et al.,

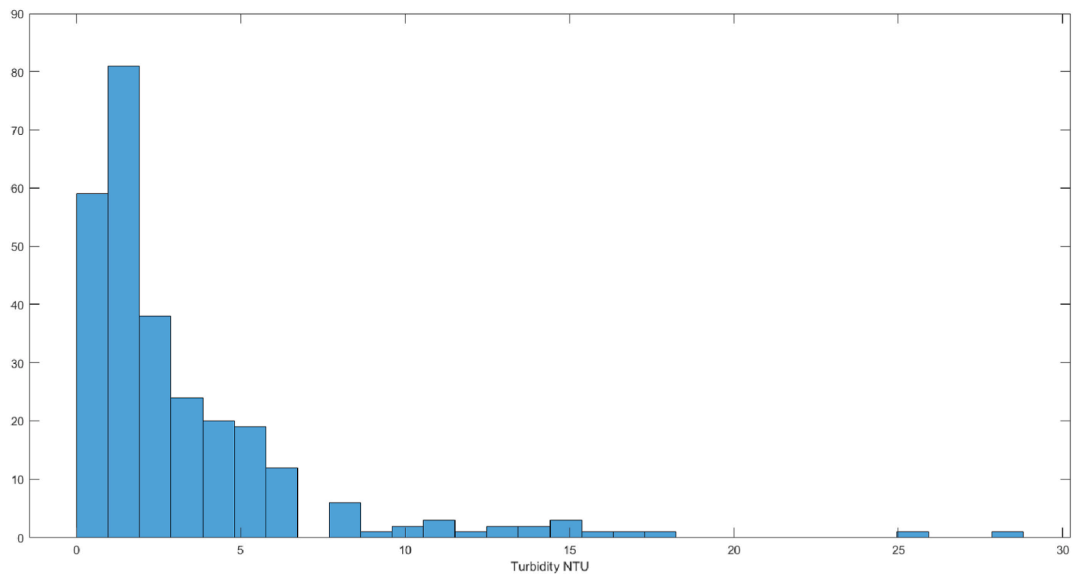

Fig. 2. Histogram of measured turbidity data distribution in NTU.

Fig. 3. An example of a True Colour Image of the study area (tile T32TNP) obtained from Level-1C Sentinel-2 MSI products (October 8th, 2020). (For interpretation of the references to colour in this figure legend, the reader is referred to the Web version of this article.)

2021). To avoid uncertainties in BOA products introduced by application of an AC method without availability of water surface radiometric data to evaluate the performance of the AC model, Level-1C TOA product was considered. The possible generation of errors related to atmospheric effect in turbidity estimates was not evaluated.

Eighty-four satellite images from April 2015 to December 2021 were analysed. Temporal resolution is indeed related to the weather conditions during the image acquisition, and cloud coverage masking must be applied to filter data and avoid wrong interpretation of the reflectance. A preventive check, to eliminate from the training set the data probably affected by the presence of clouds, which behave as outliers, can be performed by specific pixel classifiers. In practice two types of cloud cover are defined: a dense and almost completely opaque (dense cloud) and a light, semi-transparent cloud (cirrus cloud). The most difficult to manage are cirrus, because they can alter the data without being clearly confirmed by visual inspection. The Sentinel L1C product contains rough pixel classification maps for both phenomena. However, there are several reliable tools available in literature which are the result of deep statistical analysis of large amounts of data, capable of classifying pixels in a multispectral image according to their type (water, soil, clouds, snow, etc.). A comprehensive review of many cloud masking algorithms for Sentinel-2 MSI images can be found in Skakun et al. (2022). The so-called *s2cloudless* algorithm (Zupanc, 2017) was chosen, which allows to get a precise cloud coverage masking for MSI images, obtained on the basis of supervised learning conducted by the authors on thousands of tiles in different operating conditions. The statistical model is based on the Gradient Boosting technique and relies on a widely used Python package such as *LightGBM* (Ke et al., 2017). No cloud shadow masking was applied. An example of the obtained contour map of cloud masked pixels, with a threshold of 50% probability, is shown in Fig. 4, overlaid with an original TCI image. The depicted contours also include the coastline, derived from openly available cartography, and the delimitation of the valid part of the image, due to the possible cut of the orbit inside the tile itself.

The threshold of 50% on cloud probability was used for the selection of valid reflectance data. The set of the 13 L1C TOA spectral bands, in all non-masked pixels corresponding to the coordinates of the sampling stations, were then used as predictors in the regression modelling.

Fig. 5 shows the boxplot of the 222 set of spectral bands values resulting after cleaning operations and representing the final predictors. The value dispersion is larger in the visible bands (B2, B3, B4), and in band B1, affected by Coastal Aerosol.

2.4. A machine learning based approach

As discussed, the use of ML techniques allows evaluating nonlinear relationships between multi-band images and in-situ turbidity measurements. Its function-free structure results in a better approach for handling complex problems without prior knowledge (Ruescas et al., 2018).

When it comes to a complex parameter such as turbidity, in coastal regions, where the effects of organic/inorganic material become more intricate, the use of non-parametric regression algorithms can be more appropriate.

Use of ML for remotely sensed optically active water quality parameters estimation has spread in recent years thanks to the advances in algorithm development, computing power, sensor systems, and higher spatial resolution data availability (Peterson et al., 2018). Among the literature, Neural Network (NN)-based approaches to retrieve turbidity have gained popularity (Chebud et al., 2012; Hafeez et al., 2019; Peterson et al., 2020) due to their robust ability to capture complex statistical trends typical of water quality remote sensing data. However, the use deep learning is still limited by the high computational costs and the amount of training

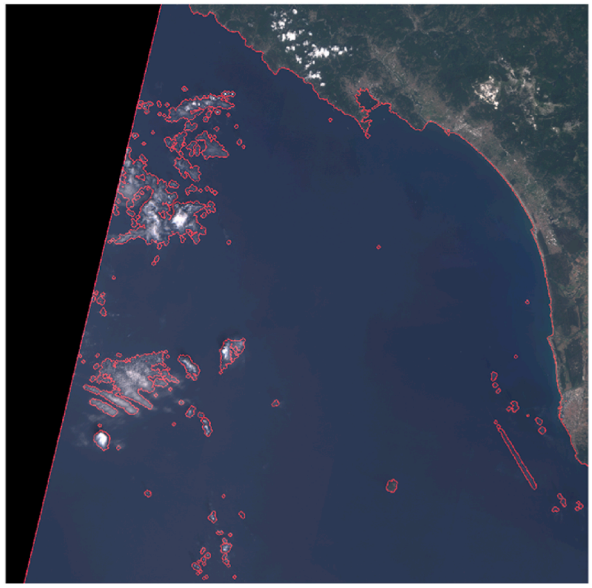

Fig. 4. Cloud masking by s2cloudless algorithm.

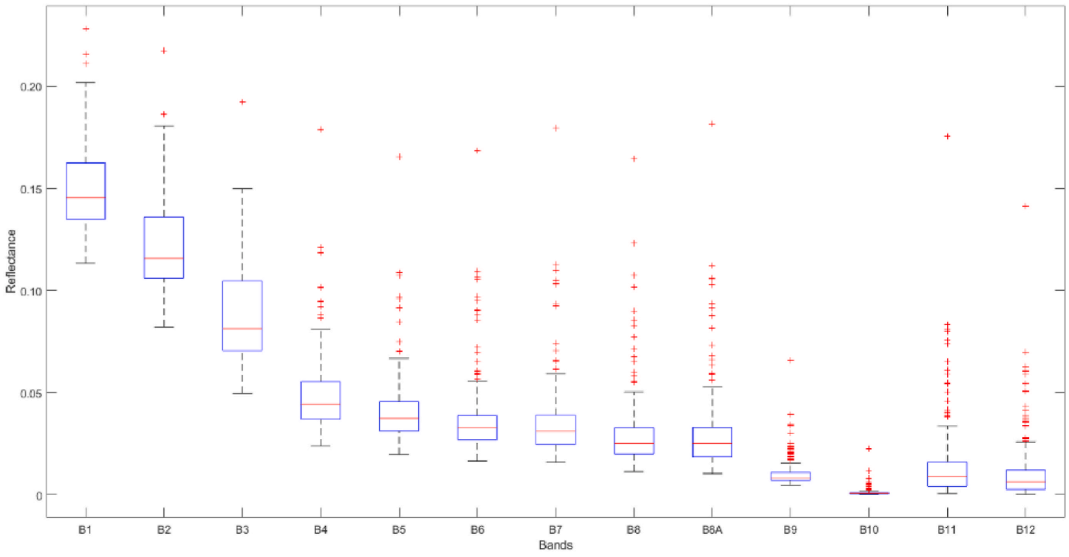

Fig. 5. Boxplot of the values of the 13 spectral bands for the 222 pixels used as predictors for turbidity estimates.

samples required to adequately calibrate the numerous parameters (Sagan et al., 2020). In the present work, two different generalized linear models, a Stepwise Linear Regression and a polynomial Kernel Regression, are proposed, characterized by a simple model structure, good generalization, global optimal solution, especially suitable for non-linear and high dimension problems.

2.5. Model implementation

In the present study, all 13 MSI bands, from L1C (TOA) Sentinel-2A/B imagery, were selected as predictive variables. After cloud mask application, a database of 222 turbidity measurements across different bio-optical regimes, ranging from 0.1 NTU to 28.7 NTU, was used to train and validate the model. Turbidity values are not normally distributed, with a median of 2.0 NTU and a mean of 3.4 NTU.

The problem of finding the model with the right complexity is referred to as model selection and the definition of the possible choices during the training process as hyperparameter tuning. The possible complexity of the model derives from the nature and number of training data. A SLR and a Kernel regression model were tested and compared.

A Leave-One-Out Cross Validation (LOOCV) procedure, a special case of K-fold cross-validation, has been used throughout the study to assess the prediction performance in an objective way (Efron, 1982). Thus, the learning algorithm is applied once for each instance, using all other instances as a training set and using the selected instance as a single-item test set.

To determine the strength of the relationships, the coefficient of determination (R^2) was used, while root mean squared error (RMSE) and the mean absolute error (MAE) were used to determine model accuracy. The Normalized Root Mean Square Error (NRMSE) and the symmetrically normalized root square error (HH) proposed by Hanna and Heinold (1985) were also calculated, applied per class of values, as these indexes have shown to provide a more reliable information than RMSE about the accuracy of the results of numerical models (Mentaschi, 2013).

The error indicator HH proposed by Hanna and Henold is defined as the RMSE divided by the absolute value of the mean of the product of the observations and modelled values:

$$HH = \sqrt{\frac{\sum_{i=1}^{N}(x_i - y_i)^2}{\sum_{i=1}^{N} y_i x_i}}$$

Finally, a comparison among turbidity estimates obtained from the developed models, data from Copernicus CMEMS dataset named 'Mediterranean Sea, Bio-Geo-Chemical, L3, daily observation', extracted for the days of the surveys in the pixel corresponding to the sampling location, and in-situ measurements was conducted.

2.5.1. Kernel method

Kernel methods provide a principled approach to nonparametric learning. The Kernel method is based on the so-called "kernel trick", that is, given a kernel function K (x, x'), symmetric and positive definite, we will implicitly have a nonlinear function $\phi(x)$ mapping the input vector x from the input space X to a new dot product space F, also called feature space, that can potentially be infinite dimensional. By using the feature map ϕ, we can classify our data by a linear model in the feature space, while the model is no longer linear in the original input space. The advantage of using such a kernel as a similarity measure is that it allows us to construct algorithms in dot product spaces.

The hyperparameters of the model are tuned by minimising the loss over the available training samples; the considered loss function is the squared loss. To ensure that the minimization problem is well defined we must add a regularisation term controlled by another hyperparameter (Meanti et al., 2022).

Polynomial kernel was used (Eq. (1)), where the degree of the polynomial *d* is a hyperparameter to be tuned.

$$K\ (x, x') = \left(x^T\ x' + c\right)^d \text{ where d} \in \text{N and c} \geq 0 \qquad \text{Eq.1}$$

The polynomial kernel of degree *d* thus computes a dot product in the space spanned by all monomials up to degree d in the input coordinates. More details on Kernel methods can be found in Hofmann et al. (2008).

2.5.2. Stepwise Linear Regression method

Stepwise linear regression (SLR) is a method of fitting linear regression models to data in which the choice of the predictive variables is carried out by an automatic procedure (James et al., 2013), relying on the incremental selection of a subset of all possible features, often enlarged by the use of a feature engineering step. The selection is performed one-by-one aiming to maximize a score function. A typical score is the adjusted R^2, which is an attempt to account for the fact that R^2 monotonically increases when extra explanatory variables are added to the model.

The main approaches for this procedure are: forward (starting from an empty subset and always adding new features to the model), backward (starting from the full initial set and sequentially removing useless features), or bidirectional (combining both types).

Apart from some criticism about the intrinsic sub-optimality of this kind of strategy (Smith, 2018), SLR coupled with knowledge-based feature engineering is a widely adopted practical way to build up simple regression models in order to highlight the most important features and combinations able to explain the variability of the target observations.

In this study, the training of the SLR model was performed by the following steps.

- augmenting the feature set including all interaction and quadratic terms
- adding the features to the model one at a time, looking for the one maximizing the adjusted R^2 after the least-square fitting
- checking for termination when adjusted R^2 does not improve further (or a maximum number of features has been reached)
- removing from the final subset all features showing poor significance, measured by the pValue < 0.05
- estimating performance of the model by LOOCV, using the predicted residual error sum of squares (PRESS) as a summary measure of the goodness of fit.

Similar results could be achieved with other sparsity-based methods like LASSO, Elastic Net or Ridge Regression (Hastie et al., 2015), however, training of these models requires a careful hyperparameter setting procedure and a copious training set.

3. Results and discussion

3.1. Turbidity model calibration

Both tested methods showed good agreement of the estimated satellite-derived surface turbidity with measured one. A 3-degree polynomial Kernel showed the best cross-validated fitting with measured data, with $R^2 = 0.725$, RMSE = 2.07 NTU and MAE = 1.40 NTU.

A SLR with 13 predictors, extracted from a pool of 104 predictors generated by feature engineering, including the original 13 bands and all interaction and quadratic terms, shows slightly better performances ($R^2 = 0.736$, RMSE = 2.03 NTU, MAE = 1.39 NTU).

Fig. 6 shows the two scatter plots depicting cross-validated turbidity (NTU) estimations vs. in situ measured values for the Kernel method (left image) and SLR (right image).

The Normalized Root Mean Square Error (NRMSE) and the symmetrically normalized root square error (HH) were calculated for the different ranges of the observed values, as shown in Table 1.

It is possible to notice that the two indexes for both methods give similar results: the Kernel method provides an average NRMSE value of 0.40 and an HH index of 0.43, while the SRL method provides an average NRMSE of 0.39 and a HH index of 0.42, with higher relative error for the lowest values of turbidity.

Fig. 7 shows the histogram of residuals in the same order. Most residuals have values in ± 2 NTU as expected, while only a few exceed this range. We noticed that samples with high residuals are nearly the same for both methods, indicating a possible problem in other stages of the data processing chain.

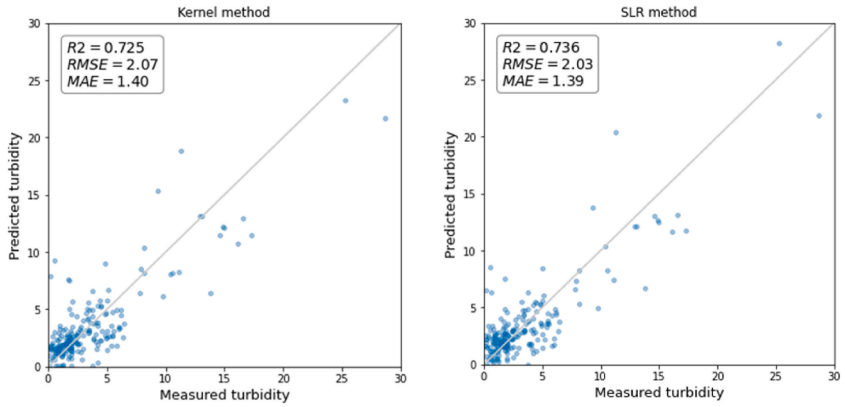

Fig. 6. Predicted vs Measured scatterplots of regression methods.

Table 1
Normalized Root Mean Square Error (NRMSE) and the symmetrically normalized root square error (HH) for different ranges of turbidity values, for the Kernel and Stepwise regression methods.

Turbidity range (NTU)	# data	NRMSE Kernel	NRMSE SLR	HH Kernel	HH SLR
0–2	114	1.26	1.25	1.07	1.06
2–5	70	0.44	0.41	0.46	0.44
5–10	23	0.41	0.40	0.45	0.46
>10	15	0.27	0.27	0.30	0.29

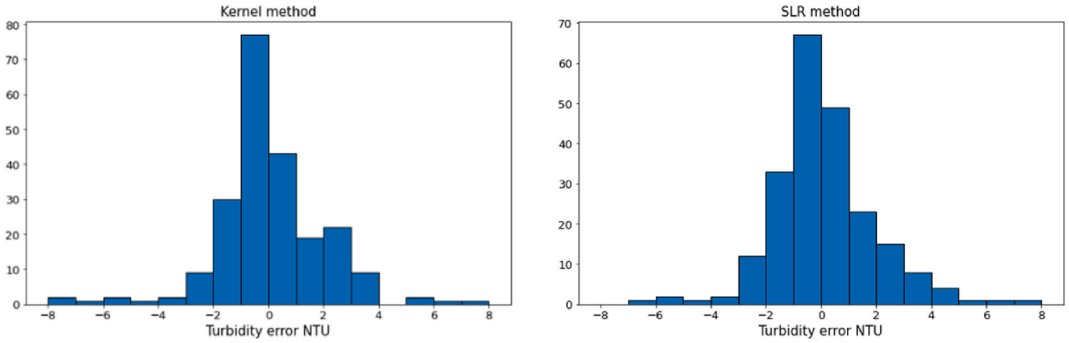

Fig. 7. Histogram of residuals of regression methods.

As these kinds of models are highly influenced by the training data, the availability of more data, especially in the less represented class (medium turbidity), is expected to improve the model accuracy.

3.2. Spectral bands' importance

A permutation analysis was conducted to estimate the relative importance of each band for the proposed predictive models: after random re-orderings (shuffling) of the predictive variable the test statistics is recalculated (Anderson and Robinson, 2001). The statistic used is the MAE and the number of runs used to achieve stable feature rankings was 30. Fig. 8 shows the increase in MAE after shuffling each of the bands: the higher the MAE value when a particular band is shuffled, the more weight it has in the model. Bands in the red-edge part of the spectrum (705–783 nm) caused a higher MAE when shuffled compared with the other bands, followed by the 865 nm (B8A) and the 665 nm (B4) bands. Bands mostly affected by atmospheric effects (Coastal-Aerosol B01, Water Vapour B09, and Cirrus B10) provide a smaller but not neglectable contribution to turbidity prediction. In general, the plot highlights the importance of widening the range of bands used for turbidity estimates.

3.3. Turbidity maps

The two models have been applied on a pixel-by-pixel basis to produce full turbidity maps of the area. An example is shown in Fig. 9 (October 8th, 2020, the same date as in Fig. 3). Such dense maps allow a direct inspection of possible high turbidity areas.

The two maps are produced at 60 m resolution, that is 1830x1830 pixels large. Higher spatial resolution could be provided resampling MSI data to a given level of detail, up to the maximum available spatial resolution of 10 m.

In the maps, a smooth transition from clear water to the turbidity peak at the mouth of river Arno is clearly visible. It is possible to see how clouds are detected and identified.

Finally, Fig. 10 shows the difference between results obtained from the two methods. In red, the areas where the SLR provides higher values than the Kernel method, while in blue where Kernel model estimates higher values. It is possible to derive that the difference between the obtained values ranges from about −2 NTU up to +3 NTU, which is in clear agreement with the results previously discussed. In particular, Kernel method tends to over-estimate to unity low values in open sea, while SLR produces higher peaks at river mouths.

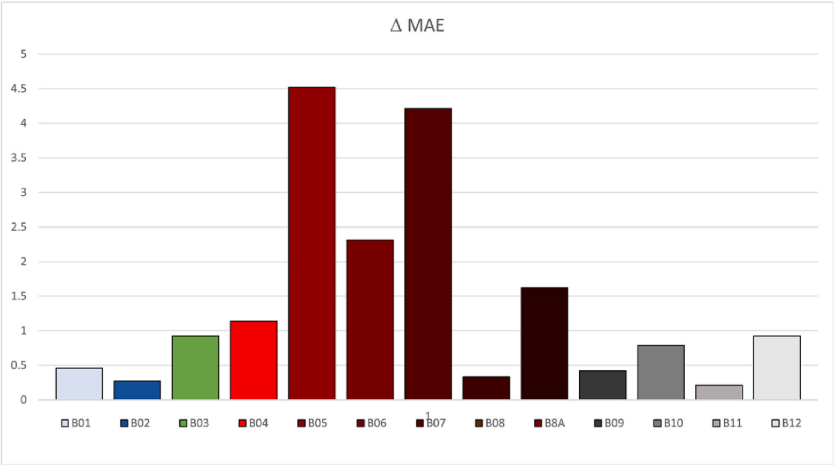

Fig. 8. Bands' importance for the proposed predictive models represented in terms of increase of MAE obtained by permutation test.

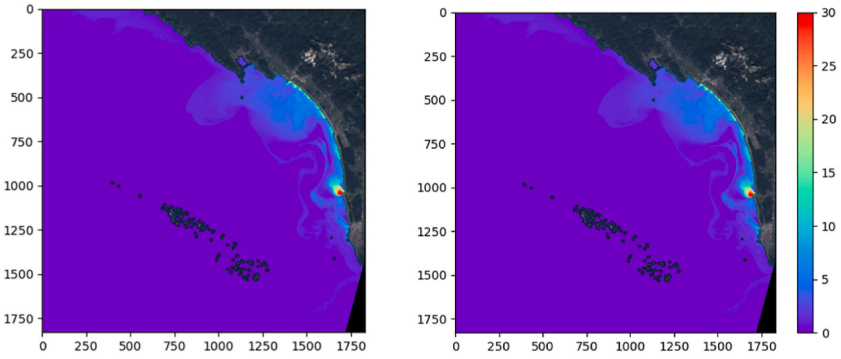

Fig. 9. Dense turbidity map in NTU obtained by the Kernel model (left image) and SLR model (right image).

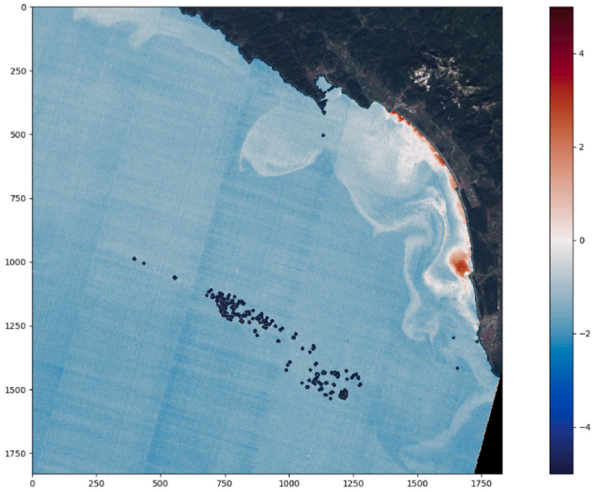

Fig. 10. Difference of turbidity values in NTU obtained by the two models.

Finally, the turbidity value of Copernicus product in the pixel corresponding to the location of the turbidity sample was extracted for the days of the surveys and compared to both the in-situ value and the estimates from the two models. Since the Copernicus product is available since January 2020, the comparison covered the period 2020–2021, including 75 turbidity values, ranging from 0.1 to 28.7 NTU. The comparison produced consistent results (Table 2).

4. Conclusions

Satellite Remote Sensing provides observations over large areas, enabling to extend the punctual information of sampling campaigns to a synoptic view. Semi-empirical polynomial algorithms have been widely used in the open ocean or inland waters. These relationships require less training data, but usually have a limited performance, spatially and temporally. ML algorithms have proved the ability to capture complex statistical trends, however, the complexity of the algorithms must consider the problem of overfitting due to the corresponding increment of parameters to be tuned, with sometimes inadequate training samples.

In the present work, two different generalized linear models, a Stepwise Linear Regression and a polynomial Kernel, were trained and validated with the available dataset of 222 combinations of turbidity measurements and TOA spectral data from Sentinel-2A/B MSI in the North Tyrrhenian Sea.

The considered area presents a wide variety of turbidity contributions and conditions, ranging from clear water (0.1 NTU) especially within the Cinque Terre Marine Protected area, to high turbidity (28.7 NTU) particularly related to sediment loads carried from rivers.

Surface turbidity derived from satellite had good agreement with measures for both proposed models ($R^2 = 0.725$, MAE = 1.40 NTU for the Kernel method, $R^2 = 0.736$, MAE = 1.39 NTU for the SLR method). That means that it is possible to predict reliable nephelometric turbidity values starting from satellite images, using the proposed methodologies. The Normalized Root Mean Square Error (NRMSE) and the symmetrically normalized root square error (HH) were also calculated and showed good results (average NRMSE value of 0.40 and an HH index of 0.43 for the Kernel method, average NRMSE of 0.39 and a HH index of 0.42 for the SRL method). Also, the consistency of results of the comparison between estimates obtained from the two proposed models with turbidity data from Copernicus CMEMS dataset named 'Mediterranean Sea, Bio-Geo-Chemical, L3, daily observation' confirms robustness of obtained turbidity estimates.

Samples with high residuals are nearly the same for both methods, in particular for medium values of turbidity, thus indicating a possible problem in other stages of the data processing chain, starting from the dataset construction itself. The daily, rather than hourly, synchronism of the in situ and satellite measurements can lead to significant differences between the turbidity values observed by the two instruments, especially during phenomena associated with an increase in suspended solids with high hydrodynamics, such as river runoff.

Table 2
Linear correlation coefficient or coefficient of determination (R^2) between in-situ measured turbidity (or ground truth - GT) in NTU, turbidity estimated from SLR and Kernel models in NTU and turbidity in FNU from the CMEMS 'Mediterranean Sea, Bio-Geo-Chemical' dataset.

	GT (NTU)	SLR (NTU)	KERNEL (NTU)	CMEMS (FNU)
GT (NTU)	1	0.885	0.868	0.852
SLR (NTU)		1	0.978	0.925
KERNEL (NTU)			1	0.946
CMEMS (FNU)				1

The use of samples collected by different operators (Liguria and Tuscany Environmental Agencies) helped achieve a more representative set for training, but, on the other hand, the lack of previous intercalibration increases the error related to the accuracy of the reference in situ data. Despite this, the model showed a good capability to generalise with respect to the used instruments, thus it is expected that new available data could be easily integrated for further calibration.

Finally, the total accuracy of the model is affected by other factors, such as probe calibration and maintenance, noise from satellite sensors and sun-glint which has higher effects in May, June and July.

The results confirm that it is possible to reach a good accuracy in turbidity estimation from satellite TOA reflectance using ML techniques. Bands ranking obtained through permutation test confirmed that all bands contribute to the model prediction and that ML techniques enhance the exploitation of all spectral information.

The two models have been applied on a pixel-by-pixel basis to produce quantitative turbidity maps from satellite imagery with different turbidity conditions, showing promising results on the flexibility of the models to operate in the entire tile area, and in different turbidity conditions than the specific training ones. The accuracy of results outside the range of the training dataset will be evaluated as more in situ data will be available. The applicability of the calibrated algorithms in other areas of the North Tyrrhenian Sea will be tested in the future, comparing results of the models with in-situ turbidity data, to evaluate whether these algorithms can be applied in close geographical sites, with supposedly similar hydrography and environments, without the need for region-specific calibration.

The potential of the model will be exploited by reconstructing historical series of turbidity in the study area to derive statistical analysis, such as seasonal or annual climatology, etc. Such results can be of crucial interest for authorities in charge of water quality monitoring, such as the Regional and National Agencies for the Environmental Protection, who will benefit from EO to integrate in situ measurements and to gather knowledge of the sea environment, and, in cascade, decision makers, such as the authorities in charge of spatial planning (e.g. for identifying areas suitable for aquaculture, for which turbidity levels represent a critical indicator).

The possibility to create historical series of turbidity, complementing existing measurements if available, can support the analysis of the relation between increase and persistence in turbidity and hydro-meteorological variables, adding important knowledge of natural seasonal turbidity fluctuations in the area. Reconstructed turbidity levels from satellite images can further lead to the identification of natural turbidity levels to be used within the Environmental Impact Assessment (EIA, Directive, 2014/52/UE) for projects that require it. Our understanding of turbidity events can be valuable in the management of the sea water quality, allowing to investigate and early detect water quality deterioration.

Ethical statement

Hereby, I, Stefania Magrì, on behalf of all authors, consciously assure that for the manuscript “Application of Machine Learning techniques to derive sea water turbidity from Sentinel-2 imagery” the following is fulfilled.

1) This material is the authors' own original work, which has not been previously published elsewhere.
2) The paper is not currently being considered for publication elsewhere.
3) The paper reflects the authors' own research and analysis in a truthful and complete manner.
4) The results are appropriately placed in the context of prior and existing research.
5) All sources used are properly disclosed (correct citation).
6) All authors have been personally and actively involved in substantial work leading to the paper and will take public responsibility for its content.
7) All ethical practices have been followed in relation to the development, writing, and publication of the article

I agree with the above statements and declare that this submission follows the policies of RSASE, as outlined in the Guide for Authors.

Authorship statement

Hereby, I, Stefania Magrì, on behalf of all authors, consciously assure that for the manuscript “Application of Machine Learning techniques to derive sea water turbidity from Sentinel-2 imagery” all persons who meet authorship criteria are listed as authors, and all authors certify that they have participated sufficiently in the work to take public responsibility for the content, including participation in the concept, design, analysis, writing, or revision of the manuscript. Furthermore, each author certifies that this material or similar material has not been and will not be submitted to or published in any other publication before its appearance in the Journal *Remote Sensing Applications: Society and Environment*.

Declaration of competing interest

The authors declare that they have no known competing financial interests or personal relationships that could have appeared to influence the work reported in this paper.

Data availability

Data will be made available on request.

Acknowledgements

Turbidity in-situ data along the Liguria and Tuscany coast were provided by the Regional Agency for the Environmental Protection of Liguria (ARPAL) and of Tuscany (ARPAT).

This work is part of the ALACRES2 Project, supported by the European Commission in the frame of the Interreg Italy-France 2014–2020 Program.

The work was in part supported by the Italian project "DRIVERS" funded by INAIL under the grant BRIC/2021/ID3.

References

Abirhire, O., Davies, J.M., Guo, X., Hudson, J., 2020. Understanding the factors associated with long-term reconstructed turbidity in Lake Diefenbaker from Landsat-imagery. Sci. Total Environ. 724, 138222. https://doi.org/10.1016/j.scitotenv.2020.138222.

Akbar, T.A., Hassan, Q.K., Achari, G., 2014. Development of remote sensing based models for surface water quality. Clean: Soil, Air, Water 42, 1044–1051. https://doi.org/10.1002/clen.201300001.

Anderson, M.J., Robinson, J., 2001. Permutation tests for linear models. Aust. N. Z. J. Stat. 43, 75–88. https://doi.org/10.1111/1467-842X.00156.

Baughman, C.A., Jones, B.M., Bartz, K.K., Young, D.B., Zimmerman, C.E., 2015. Reconstructing turbidity in a glacially influenced lake using the landsat TM and ETM+ surface reflectance climate data record archive, lake Clark, Alaska. Rem. Sens. 7, 13692–13710. https://doi.org/10.3390/rs71013692.

Binding, C.E., Pizzolato, L., Zeng, C., 2021. EOLakeWatch; delivering a comprehensive suite of remote sensing algal bloom indices for enhanced monitoring of Canadian eutrophic lakes. Ecol. Indicat. 121. https://doi.org/10.1016/j.ecolind.2020.106999.

Bustamante, J., Pacios, F., Díaz-Delgado, R., Aragonés, D., 2009. Predictive models of turbidity and water depth in the Doñana marshes using Landsat TM and ETM+ images. J. Environ. Manag. 90 (7), 2219–2225. https://doi.org/10.1016/j.jenvman.2007.08.021.

Caballero, I., Steinmetz, F., Navarro, G., 2018. Evaluation of the first year of operational sentinel-2A data for retrieval of suspended solids in medium- to high-turbidity waters. Rem. Sens. 10, 982. https://doi.org/10.3390/rs10070982.

Chebud, Y., Naja, G., Rivero, R., Melesse, A., 2012. Water quality monitoring using remote sensing and an artificial neural network. Water, air. & Soil Pollution 223, 4875–4887. https://doi.org/10.1007/s11270-012-1243-0.

Chen, Z., Hu, C., Muller-Karger, F., 2007. Monitoring turbidity in Tampa bay using MODIS/Aqua250m imagery. Remote Sens. Environ. 109 (2), 207–220. https://doi.org/10.1016/j.rse.2006.12.019.

Chu, H.J., Kong, S.J., Chang, C.H., 2018. Spatio-temporal water quality mapping from satellite images using geographically and temporally weighted regression. Int. J. Appl. Earth Obs. Geoinf. 65, 1–11. https://doi.org/10.1016/j.jag.2017.10.001.

Copernicus Open Access Hub website, accessed November 2022.

Dogliotti, A.I., Ruddick, K.G., Nechad, B., Doxaran, D., Knaeps, E., 2015. A single algorithm to retrieve turbidity from remotely-sensed data in all coastal and estuarine waters. Remote Sens. Environ. 156, 157–168. https://doi.org/10.1016/j.rse.2014.09.020.

Doxaran, D., Froidefond, J.M., Castaing, P., 2002. A reflectance band ratio used to estimate suspended matter concentrations in sediment-dominated coastal waters. Int. J. Rem. Sens. 23, 5079–5085. https://doi.org/10.1080/0143116021000009912.

Doxaran, D., Froidefond, J., Lavender, S., Castaing, P., 2002b. Spectral signature of highly turbid waters Application with SPOT data to quantify suspended particulate matter concentrations. Remote Sens. Environ. 81, 149–161. https://doi.org/10.1016/S0034-4257(01)00341-8.

Doxaran, D., Froidefond, J., Castaing, P., Babin, M., 2009. Dynamics of the turbidity maximum zone in a macrotidal estuary (the Gironde, France): observations from field and MODIS satellite data. Estuar. Coast Shelf Sci. 81, 321–332. https://doi.org/10.1016/j.ecss.2008.11.013.

Efron, B., 1982. The Jackknife, the Bootstrap and other resampling plans. In: CBMS-NSF Regional Conference Series in Applied Mathematics 1982. Philadelphia, PA.

El Din, E.S., 2019. Enhancing the accuracy of retrieving quantities of turbidity and total suspended solids using Landsat-8-based-principal component analysis technique. J. Spat. Sci. 66 (3), 493–512. https://doi.org/10.1080/14498596.2019.1674197.

Erftemeijer, P.L.A., Riegl, B., Hoeksema, B.W., Todd, P.A., 2012. Environmental impacts of dredging and other sediment disturbances on corals: a review. Mar. Pollut. Bull. 64, 1737–1765. https://doi.org/10.1016/j.marpolbul.2012.05.008.

Feng, L., Hu, C., Chen, X., Song, Q., 2014. Influence of the three gorges dam on total suspended matters in the yangtze estuary and its adjacent coastal waters: observations from MODIS. Remote Sens. Environ. 140, 779–788. https://doi.org/10.1016/j.rse.2013.10.002.

Garbolino, E., Aqua, J., Abriak, N., 2014. Applicability of H14 protocol for sediments in order to consider their valorization: limits and benefits. Chem. Eng. Trans. 36, 631–636. https://doi.org/10.3303/CET1436106.

Hafeez, S., Wong, M.S., Ho, H.C., Nazeer, M., Nichol, J., Abbas, S., Tang, D., Lee, K.H., Pun, L., 2019. Comparison of machine learning algorithms for retrieval of water quality indicators in case-II waters: a case study of Hong Kong. Rem. Sens. 11, 617. https://doi.org/10.3390/rs11060617.

Han, B., Loisel, H., Vantrepotte, V., Mériaux, X., Bryère, P., Ouillon, S., Dessailly, D., Xing, Q., Zhu, J., 2016. Development of a semi-analytical algorithm for the retrieval of suspended particulate matter from remote sensing over clear to very turbid waters. Rem. Sens. 8, 211. https://doi.org/10.3390/rs8030211.

Hanna, S.R., Heinold, D.W., 1985. Development and application of a simple method for evaluating air quality models. API Pub 4409.

Hastie, T., Tibshirani, R., Wainwright, M., 2015. Statistical Learning with Sparsity: the Lasso and Generalisations. Chapman & Hall/CRC.

Hofmann, T., Schölkopf, B., Smola, A.J., 2008. Kernel methods in machine learning. Ann. Stat. 36 (3), 1171–1220. https://doi.org/10.1214/009053607000000677.

Hudson, A.S., Talke, S.A., Jay, D.A., 2017. Using satellite observations to characterize the response of estuarine turbidity maxima to external forcing. Estuaries coasts. Estuar. Coast 40, 343–358. https://doi.org/10.1007/s12237-016-0164-3.

James, G., Witten, D., Hastie, T., Tibshirani, R., 2013. An Introduction to Statistical Learning with Applications in R, 103. Springer.

Joshi, I.D., D'Sa, E.J., Osburn, C.L., Bianchi, T.S., 2017. Turbidity in apalachicola bay, Florida from landsat 5 TM and field data: seasonal patterns and response to extreme events. Rem. Sens. 9 (4), 367. https://doi.org/10.3390/rs9040367.

Katlane, R., Dupouy, C., El Kilani, B., Berges, J.C., 2020. Estimation of chlorophyll and turbidity using Sentinel 2A and EO1 data in kneiss archipelago gulf of gabes, Tunisia. Int. J. Geosci. 11, 708–728. https://doi.org/10.4236/ijg.2020.1110035.

Ke, G., Meng, Q., Finley, T., Wang, T., Chen, W., Ma, W., Ye, Q., Liu, T.Y., 2017. LightGBM: a highly efficient gradient boosting decision tree. Adv. Neural Inf. Process. Syst. 30 (NIPS). 2017.

Kirk, J.T.O., 1985. Effects of suspensoids (turbidity) on penetration of solar radiation in aquatic ecosystems. Hydrobiologia 125, 195–208. https://doi.org/10.1007/BF00045935.

Lisi, I., Feola, A., Bruschi, A., Pedroncini, A., Pasquali, D., Di Risio, M., 2019. Mathematical modeling framework of physical effects induced by sediments handling operations in marine and coastal areas. J. Mar. Sci. Eng. 7, 149. https://doi.org/10.3390/jmse7050149.

Liu, L.W., Wang, Y.M., 2019. Modelling reservoir turbidity using landsat 8 satellite imagery by gene expression programming. Water 11 (7), 1479. https://doi.org/10.3390/w11071479.

Magrì, S., De Gaetano, P., Feola, A., Lisi, I., Salmeri, A., Venti, F., Pedroncini, A., 2020. Numerical modelling for environmental impact assessment of sediment dispersion in port areas. Comput. Aided Chem. Eng. 48, 337–342. https://doi.org/10.1016/B978-0-12-823377-1.50057-4.

Meanti, G., Carratino, L., De Vito, E., Rosasco, L., 2022. Efficient Hyperparameter Tuning for Large Scale Kernel Ridge Regression. https://doi.org/10.48550/arXiv.2201.06314. arXiv.

Medina-Lopez, E., 2020. Machine learning and the end of atmospheric corrections: a comparison between high-resolution Sea Surface salinity in coastal areas from Top and bottom of atmosphere sentinel-2 imagery. Rem. Sens. 12, 2924. https://doi.org/10.3390/rs12182924.

Mentaschi, L., Besio, G., Cassola, F., Mazzino, A., 2013. Problems in RMSE-based wave model validations. Ocean Model. 72, 53–58. https://doi.org/10.1016/j.ocemod.2013.08.003.

Miller, R.L., McKee, B.A., 2004. Using MODIS Terra 250 m imagery to map concentrations of total suspended matter in coastal waters. Remote Sens. Environ. 93,

259–266. https://doi.org/10.1016/j.rse.2004.07.012.
Nas, B., Ekercin, S., Karabörk, H., Berktay, A., Mulla, D.J., 2010. An application of landsat-5 TM image data for water quality mapping in lake beysehir, Turkey. Water Air Soil Pollut. 212, 183–197. https://doi.org/10.1007/s11270-010-0331-2.
Nechad, B., Ruddick, K.G., Park, Y., 2010. Calibration and validation of a generic multisensor algorithm for mapping of total suspended matter in turbid waters. Remote Sens. Environ. 114, 854–866. https://doi.org/10.1016/j.rse.2009.11.022.
Novoa, S., Doxaran, D., Ody, A., Vanhellemont, Q., Lafon, V., Lubac, B., Gernez, P., 2017. Atmospheric corrections and multi-conditional algorithm for multi-sensor remote sensing of suspended particulate matter in low-to-high turbidity levels coastal waters. Rem. Sens. 9, 61. https://doi.org/10.3390/rs9010061.
OSPAR Commission, 2008. Marine Biodiversity Monitoring and Assessment: Activities to Improve Synergies between EU Directives and International Convention, 357. Publication, ISBN 978-1-905859-96-2. 2008.
Pahlevan, N., Smith, B., Schalles, J., Binding, C., Cao, Z., Ma, R., Alikas, K., Kangro, K., Gurlin, D., Hà, N., Matsushita, B., Moses, W., Greb, S., Lehmann, M.K., Ondrusek, M., Oppelt, N., Stumpf, R., 2020. Seamless retrievals of chlorophyll-a from Sentinel-2 (MSI) and Sentinel-3 (OLCI) in inland and coastal waters: a machine-learning approach. Remote Sens. Environ. 240. https://doi.org/10.1016/j.rse.2019.111604.
Pahlevan, N., Mangin, A., Balasubramanian, S.V., Smith, B., Alikas, K., Arai, K., Barbosa, C., Bélanger, S., Binding, C., Bresciani, M., Giardino, C., Gurlin, D., Fan, Y., Harmel, T., Hunter, P., Ishikaza, J., Kratzerv, Lehmann M.K., Ligi, M., Ma, R., Martin-Lauzer, F.-R., Olmanson, L., Oppelt, N., Pan, Y., Peters, S., Reynaud, N., Sander de Carvalho, L.A., Simis, S., Spyrakos, E., Steinmetz, F., Stelzer, K., Sterckx, S., Tormos, T., Tyler, A., Vanhellemont, Q., Warren, M., 2021. ACIX-Aqua: a global assessment of atmospheric correction methods for Landsat-8 and Sentinel-2 over lakes, rivers, and coastal waters. Remote Sens. Environ. 258, 112366. https://doi.org/10.1016/j.rse.2021.112366.
Pereira, L.S.F., Andes, L.C., Cox, A.L., Ghulam, A., 2018. Measuring suspended-sediment concentration and turbidity in the middle Mississippi and lower Missouri rivers using landsat data. JAWRA 54 (2), 440–450. https://doi.org/10.1111/1752-1688.12616.
Peterson, K.T., Sagan, V., Sidike, P., Cox, A.L., Martinez, M., 2018. Suspended sediment concentration estimation from landsat imagery along the Lower Missouri and Middle Mississippi rivers using an extreme learning machine. Rem. Sens. 10, 1503. https://doi.org/10.3390/rs10101503.
Peterson, K.T., Sagan, V., Sloan, J., 2020. Deep learning-based water quality estimation and anomaly detection using Landsat-8/Sentinel-2 virtual constellation and cloud computing. GIScience Remote Sens. https://doi.org/10.1080/15481603.2020.1738061.
Petus, C., Chust, G., Gohin, F., Doxaran, D., Froidefond, J.M., Sagarminaga, Y., 2010. Estimating turbidity and total suspended matter in the Adour River plume (South Bay of Biscay) using MODIS 250-m imagery. Continent. Shelf Res. 30, 379–392. https://doi.org/10.1016/j.csr.2009.12.007.
Pisanti, A., Magrì, S., Ferrando, I., Federici, B., 2022. Seawater turbidity analysis from Sentinel-2 images: atmospheric correction and bands correlation. Int. Arch. Photogram. Rem. Sens. Spatial Inf. Sci. 371–378. https://doi.org/10.5194/isprs-archives-XLVIII-4-W1-2022-371-2022. XLVIII-4/W1-2022.
Quang, N.H., Sasaki, J., Higa, H., Huan, N.H., 2017. Spatiotemporal variation of turbidity based on landsat-8 OLI in cam ranh bay and thuy trieu lagoon. Vietnam. Water 9 (8), 570. https://doi.org/10.3390/w9080570.
Ruescas, A.B., Hieronymi, M., Mateo-Garcia, G., Koponen, S., Kallio, K., Camps-Valls, G., 2018. Machine learning regression approaches for colored dissolved organic matter (CDOM) retrieval with S2-MSI and S3-OLCI simulated data. Rem. Sens. 10, 786. https://doi.org/10.3390/rs10050786.
Sagan, V., Peterson, K.T., Maimaitijiang, M., Sidike, P., Sloan, J., Greeling, B.A., 2020. Monitoring inland water quality using remote sensing: potential and limitations of spectral indices, bio-optical simulations, machine learning, and cloud computing. Earth Sci. Rev. 103187. https://doi.org/10.1016/j.earscirev.2020.103187.
Skakun, S., Wevers, J., Brockmann, C., Doxani, G., Aleksandrov, M., Batič, M., Frantz, D., Gascon, F., Gómez-Chova, L., Hagolle, O., López-Puigdollers, D., Louis, J., Lubej, M., Mateo-García, G., Osman, J., Peressutti, D., Pflug, B., Puc, J., Richter, R., Roger, J.C., Scaramuzza, P., Vermote, E., Vesel, N., Zupanc, A., Žust, L., 2022. Cloud Mask Intercomparison eXercise (CMIX): an evaluation of cloud masking algorithms for Landsat 8 and Sentinel-2. Remote Sens. Environ. 274. https://doi.org/10.1016/j.rse.2022.112990.
Smith, G., 2018. Step away from stepwise. Journal of Big Data 5, 32. https://doi.org/10.1186/s40537-018-0143-6.
Wilber, D.H., Clark, D.G., 2001. Biological effects of suspended sediments: a review of suspended sediment impacts on fish and shellfish with relation to dredging activities in estuaries. N. Am. J. Fish. Manag. 21 (4), 855–875. https://doi.org/10.1577/1548-8675.
Zampoukas, N., Piha, H., Bigagli, E., Hoepffner, N., Hanke, G., Cardoso, A.C., 2012. Monitoring for the Marine Strategy Framework Directive: Requirements and Options. Joint Research Centre, Institute for Environment and Sustainability Publications Office. https://doi.org/10.2788/77640.
Zampoukas, N., Piha, H., Bigagli, E., Hoepffner, N., Hanke, G., Cardoso, A., 2013. Marine monitoring in the European Union: how to fulfill the requirements for the marine strategy framework directive in an efficient and integrated way. Mar. Pol. 39, 349–351. https://doi.org/10.1016/j.marpol.2012.12.004.
Zupanc, A., 2017. Improving Cloud Detection with Machine Learning. Accessed 2021. https://medium.com/sentinel-hub/improving-cloud-detection-with-machine-learning-c09dc5d7cf13.